View metadata, citation and similar papers at core.ac.uk

brought to you by CORE

provided by Hydraulic Engineering Repository

HENRY

Hydraulic Engineering Repository

Ein Service der Bundesanstalt für Wasserbau

Conference Paper, Published Version

Goethel, O.; Zielke, Werner

A Model of Scouring around Structures including Stability Analysis of the Bottom

Verfügbar unter/Available at: https://hdl.handle.net/20.500.11970/100021

Vorgeschlagene Zitierweise/Suggested citation:
Goethel, O.; Zielke, Werner (2006): A Model of Scouring around Structures including Stability Analysis of the Bottom. In: Verheij, H.J.; Hoffmans, Gijs J. (Hg.): Proceedings 3rd International Conference on Scour and Erosion (ICSE-3). November 1-3, 2006, Amsterdam, The Netherlands. Gouda (NL): CURNET. S. 240-245.

Standardnutzungsbedingungen/Terms of Use:

Die Dokumente in HENRY stehen unter der Creative Commons Lizenz CC BY 4.0, sofern keine abweichenden Nutzungsbedingungen getroffen wurden. Damit ist sowohl die kommerzielle Nutzung als auch das Teilen, die Weiterbearbeitung und Speicherung erlaubt. Das Verwenden und das Bearbeiten stehen unter der Bedingung der Namensnennung. Im Einzelfall kann eine restriktivere Lizenz gelten; dann gelten abweichend von den obigen Nutzungsbedingungen die in der dort genannten Lizenz gewährten Nutzungsrechte.

Documents in HENRY are made available under the Creative Commons License CC BY 4.0, if no other license is applicable. Under CC BY 4.0 commercial use and sharing, remixing, transforming, and building upon the material of the work is permitted. In some cases a different, more restrictive license may apply; if applicable the terms of the restrictive license will be binding.

A Model of Scouring around Structures including Stability Analysis of the Bottom

O. Goethel*, W. Zielke*
* University of Hannover, Hannover, Germany

I. Introduction

When the process of scouring is examined in a numerical model, flow and sediment transport are simulated in order to achieve knowledge of the temporal evolution and final scour depth. The modeling is limited to fluid flow, sediment transport at the bottom surface layer and resulting bottom evolution. Additional bottom movements are reduced to sliding sediment at the developing slopes. Less attention has until now been drawn to the modeling of the inner stability and the response of the bottom to shear stress and sediment transport. In order to gain more knowledge about the bottom and its behavior while the scouring process takes place, a finite element model for solids was implemented. The bottom surface geometry resulting from the sediment transport and the near-bed shear stress are taken into account as boundary conditions.

II. Model Description

A. Flow

To simulate a scouring processs the sediment transport model needs the input from a flow model, which calculates the near-bed shear stresses. Considering a cylinder in a steady current, the relevant flow effects for the scouring process are the horseshoe vortex, the increased flow velocities at the side of the pile and the vortex shedding. Especially the horseshoe vortex is a truly three-dimensional flow effect and therefore the incompressible Reynolds-averaged Navier-Stokes equations are solved for all three dimensions. Turbulence modeling is done by the k-ω model derived by [22]. The modifications of [10] were applied because of their advantage in simulating flow with a boundary layer and adverse pressure gradients.

The Reynolds equations are solved on a mesh of prismatic elements, which are obtained by duplicating a two-dimensional base mesh of triangles in the vertical direction. The mesh is refined in the vicinity of the cylinder and near the bottom, so that element edges have a minimum length of 1mm. Diffusion terms are solved implicitly and advection is done by the streamline upwind Petrov-Galerkin method [6].

B. Sediment Transport

The sediment transport is calculated as bed-load transport, which takes place at the bottom surface. In order to calculate a new bottom geometry, the bottom evolution equation (1) is being solved. The data for the necessary transport rate in (1) is determined by solving (2), which was found by [19].

$$\frac{\partial z_B}{\partial t} + \mathrm{div}\vec{q}_S = 0 \tag{1}$$

$$q_S = 0.25 d_{50} U_f D_*^{-0.3} \left(\frac{\tau - \tau_{cr}}{\tau_{cr}} \right) \tag{2}$$

$$\text{with } D_* = \left[\frac{(\rho_S / \rho - 1) g}{\nu^2} \right]^{1/3} d_{50} \tag{3}$$

D_* is a dimensionless particle parameter in which ν is the kinematic viscosity and d_{50} the medium grain diameter. In (2) U_f is the effective bed-shear velocity.

Sediment transport takes place, when the actual shear stress exceeds a critical value which can be expressed by the Shields mobility parameter θ_{cr} [15]. This is calculated by a parametrization of the Shields curve (4) done by [19]. Shear stress and mobility parameter are related by $\tau = \theta(\rho_S - \rho) g d_{50}$.

Steep slopes will occur as the scour developes, whereas most transport rate equations were derived for nearly horizontal beds. Experimental data shows that the transport rate [16] and threshold conditions change on a sloping bed. The differing values are caused by the influence of gravity on the sediment particles (Fig. 1). Therefore a correction of sediment transport rate and mobility parameter has to be done in order to take the slope effect into account.

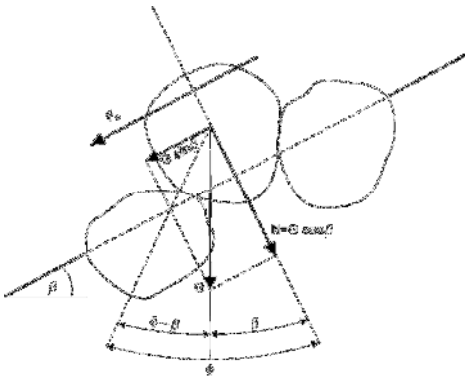

Figure 1. Sediment Particles on a Slope

The result for the Shields parameter on a horizontal bed is adjusted by (6) and (7) for longitudinal and transversal slopes based on the direction of the bed-shear velocity. Equation (6) was derived from the equilibrium of forces on a single particle on a sloping bed and was first presented by [13]. Comparison with experimental data shows good agreements [21]. The adjustment of the critical Shields parameter for transversal slopes (7) was first presented by [8] and was also derived by [7] and [3]. In (6) and (7) φ is the angle of repose and β is the actual slope angle.

$$\begin{aligned}
\theta_{cr} &= 0.24D_*^{-1} && \text{for} && 1 < D_* \le 4 \\
\theta_{cr} &= 0.14D_*^{-0.64} && \text{for} && 4 < D_* \le 10 \\
\theta_{cr} &= 0.04D_*^{-0.1} && \text{for} && 10 < D_* \le 20 \\
\theta_{cr} &= 0.013D_*^{-0.29} && \text{for} && 20 < D_* \le 150 \\
\theta_{cr} &= 0.055 && \text{for} && D_* > 150
\end{aligned} \tag{4}$$

$$\theta_{cr,slope} = \alpha_L \alpha_T \theta_{cr} \tag{5}$$

$$\alpha_L = \sin(\varphi - \beta_L)/\sin\varphi \tag{6}$$

$$\alpha_T = \cos\beta_T \left[1 - \tan^2\beta_T / \tan^2\varphi\right]^{0.5} \tag{7}$$

The sediment transport rate is treated in a smiliar way as the mobility parameter. Increasing the transport rate on a downward slope is taken into account by different equations for a longitudinal and a transversal slope. Equation (8) was found by [19] based on the equation of [16]. It predicts the amplification of the transport rate for a slope with decreasing elevation. In (8) C is the Chézy coefficient.

$$k_L = 0.5g^{-0.5}\left(\frac{d_{90}}{d_{30}}\right)^{0.2} C\tan^{0.6}\beta_L \left(\frac{\tau_b}{(\tau_b - \tau_{b,cr})}\right)^{0.5} \tag{8}$$

For slopes with increasing elevation no correction of the sediment transport rate is done. From experiments [1] found that the bed-load on an upward slope is adequately described by taking into account the modification of the critical Shields parameter.

The bed-load transport in the transverse direction was studied by [2], [4], [5] and [14]. The approach of [4] was chosen and implemented in the sediment transport model. The transport rate in cross direction is described by:

$$q_{s,T} = \left[\tan(u_{b,T}/u_{b,L}) + 1.5\left(\frac{\tau_{cr}}{\tau}\right)^{0.5} \tan\left(\frac{\partial z_B}{\partial T}\right)\right] \tag{9}$$

in which u_b is the near-bed velocity.

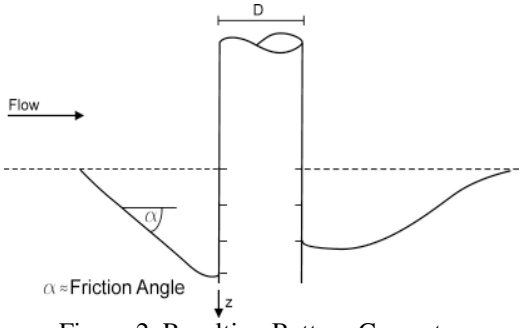

Figure 2. Resulting Bottom Geometry

When the scour develops in a sandy bed and the slope angle reaches the angle of repose, the slope will destabilize and sediment slides down in direction of the highest gradient. This effect must be taken into account in order to obtain a reasonable bottom geometry. The effect was implemented in a numerical model by initiating a sediment transport in direction of the gradient if the slope angle exceeds the angle of repose [11][12]. Hence the bottom evolution equation needs to be solved when a sandslide is executed. Sediment transport stops when the slope angle falls below the angle of repose. A slightly different way to model a sandslide is to shift the sediment in a mass conservative way from the higher meshpoints to the lower [20]. The criterion for initiating and stopping a sandslide is again the angle of repose. The resulting bottom geometry is therefore limited to the choice of this soil parameter (Fig. 2).

C. Bottom

Modeling the bottom with a finite element model provides the oppurtunity to examine its response to a changing geometry and to the shear stresses affecting the surface layer. The developing scour leads to steep slopes which become unstable when the angle of repose is reached. With the finite element model the mentioned behaviour can be simulated. Location and depth of instabilities can be analyzed.

The finite element model includes a linear-elastic as well as a visco-plastic (initial strain) method [23] with the failure criterions of Mohr-Coulomb and von Mises. In both cases the equations for equilibrium (10), strain-displacement relation (12) and the constitutive soil model are solved (11).

$$\begin{aligned}
\frac{\partial\sigma_x}{\partial x} + \frac{\partial\tau_{xy}}{\partial y} + \frac{\partial\tau_{xz}}{\partial z} &= 0 \\
\frac{\partial\sigma_y}{\partial y} + \frac{\partial\tau_{xy}}{\partial x} + \frac{\partial\tau_{yz}}{\partial z} &= 0 \\
\frac{\partial\sigma_z}{\partial z} + \frac{\partial\tau_{xz}}{\partial x} + \frac{\partial\tau_{yz}}{\partial y} &= 0
\end{aligned} \tag{10}$$

$$\begin{Bmatrix}\sigma_x\\ \sigma_y\\ \sigma_z\end{Bmatrix}=\frac{E}{1-\nu^2}\begin{bmatrix}1 & \nu & \nu\\ \nu & 1 & \nu\\ \nu & \nu & 1\end{bmatrix}\begin{Bmatrix}\varepsilon_x\\ \varepsilon_y\\ \varepsilon_z\end{Bmatrix}$$

$$\begin{Bmatrix}\tau_{xy}\\ \tau_{yz}\\ \tau_{xz}\end{Bmatrix}=\frac{E}{1-\nu^2}\begin{bmatrix}\frac{1-\nu}{2} & 0 & 0\\ 0 & \frac{1-\nu}{2} & 0\\ 0 & 0 & \frac{1-\nu}{2}\end{bmatrix}\begin{Bmatrix}\gamma_x y\\ \gamma_{yz}\\ \gamma_{xz}\end{Bmatrix} \qquad (11)$$

$$\begin{Bmatrix}\varepsilon_x\\ \varepsilon_y\\ \varepsilon_z\\ \gamma_{xy}\\ \gamma_{yz}\\ \gamma_{xz}\end{Bmatrix}=\begin{bmatrix}\frac{\partial}{\partial x} & & \\ & \frac{\partial}{\partial y} & \\ & & \frac{\partial}{\partial z}\\ \frac{\partial}{\partial y} & \frac{\partial}{\partial x} & \\ & \frac{\partial}{\partial z} & \frac{\partial}{\partial y}\\ \frac{\partial}{\partial z} & & \frac{\partial}{\partial x}\end{bmatrix}\begin{Bmatrix}u\\ v\\ w\end{Bmatrix} \qquad (12)$$

In (10)-(12) σ and τ are the stress components, ε and γ are the strains and (u,v,w) are the displacements. The soil paramters E and ν denote Young's modulus and Poisson's ratio. Solving (10)-(12) on a finite element mesh leads to a linear system of equations.

The case of a collapsing slope or sand slide is not an elastic problem. Irrecoverable strains occur when a failure of soil material takes place. In order to separate stresses causing elastic from those causing plastic deformations, a yield surface (failure criterion) is defined. For frictional materials, such as sand, the Mohr-Coulomb criterion can be applied. It has the form of an irregular hexagonal cone, as shown in Fig. 3.

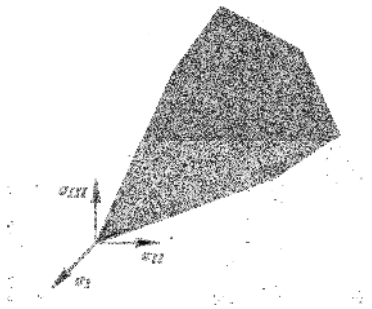

Figure 3. Mohr-Coulomb Yield Surface

The failure criterion is then given by

$$F=\sigma_m\sin\varphi+\bar{\sigma}\left(\frac{\cos\theta}{\sqrt{3}}-\frac{\sin\theta\sin\varphi}{3}\right)-c\cos\varphi\,. \qquad (13)$$

The friction angle is denoted with φ and c is the cohesion. The three invariants σ_m, $\bar{\sigma}$ and θ represent the mean stress, the deviator stress and the Lode angle.

$$\sigma_m=\sigma_x+\sigma_y+\sigma_z \qquad (14)$$

$$\bar{\sigma}=\left[(\sigma_x-\sigma_y)^2+(\sigma_y-\sigma_z)^2+(\sigma_z-\sigma_x)^2+6\tau_{xy}^2+6\tau_{yz}^2+6\tau_{xz}^2\right]^{0.5} \qquad (15)$$

$$\theta=1/3\left(\frac{-3\sqrt{6}J_3}{(\bar{\sigma}\sqrt{3})^3}\right) \qquad (16)$$

The invariants (14)-(16) are related to the principal stress space through:

$$\begin{aligned}\sigma_1&=\sigma_m+2/3\bar{\sigma}\sin(\theta-2/3\pi)\\ \sigma_2&=\sigma_m+2/3\bar{\sigma}\sin(\theta+2/3\pi)\\ \sigma 3&=\sigma_m+2/3\bar{\sigma}\sin\theta\end{aligned} \qquad (17)$$

The non-linearity of the process is taken into account by iteratively modifying the load vector and keeping the stiffness matrix constant. Each iteration is a linear-elastic analysis as described above. The plastic parts of the result are self-equilibrating loads which are applied to the load vector to redistribute the stress within the system [17].

The bottom surface geometry exists as a mesh of triangles. In order to obtain a three-dimensional mesh, a horizontal layer of triangles with the same element coordinates as the surface layer is created (Fig. 4). It is located 20% underneath the height of the lowest surface mesh point. The Space in between those layers is filled with a constant number of prismatic elements in the vertical direction.

The bottom finite element model has different degrees of freedom at the boundaries. No displacements are allowed at the bottom layer, whereas the surrounding boundary faces and the nodes at the cylinder are allowed to move in vertical direction.

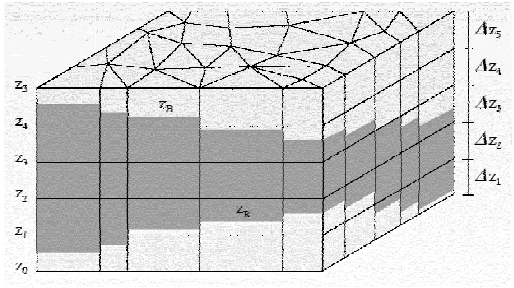

Figure 4. Bottom Mesh Structure [9]

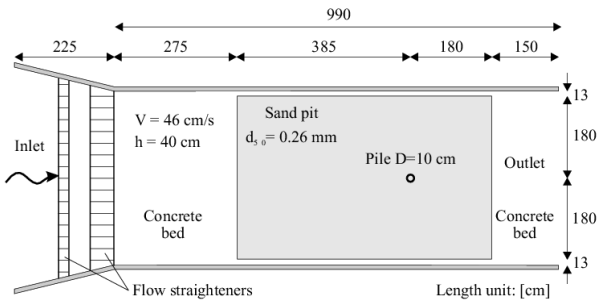

Figure 5. Scour Experiment [11]

III. MODELING RESULTS

A. *Flow and Scour*

The experimental results of [11] were used for verification of the flow and sediment transport model. The experiments were carried out in a flume with a width of 3.6m and a length of 9.90m (Fig. 5). A cylinder with a diameter of 10cm was placed within the sand pit. The sediment particles had a medium diameter of 0.26mm and the undisturbed flow velocity was 0.46cm/s at a water depth of 0.4m. The angle of repose for the given material wa defined as 32 degrees.

The flow around a vertical pile leads to vortex shedding (Fig. 6), known as the von Karman vortex street, and the horseshoe vortex (Fig. 7). The latter is caused by the difference in the vertical pressure, which occurs when a flow with a logarithmic velocity profile approaches the cylinder. Both flow effects are reproduced by the numerical model. The influence of the horseshoe vortex on the direction of the near-bed flow velocities can be seen in Fig. 8. In the upstream part of the cylinder the near-bed velocity points against the direction of the approaching flow. The contraction of the flow leads to increased velocities at the cylinder sides and therefore to an increased shear stress. In the numerical simulations the maximum value reaches eight times of that in the undisturbed areas as can be seen in Fig. 9.

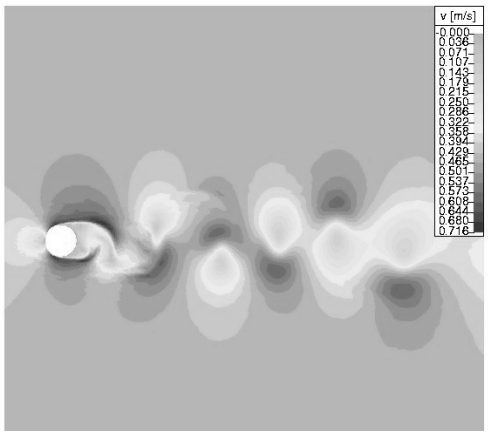

Figure 6. von Karman Vortex Street

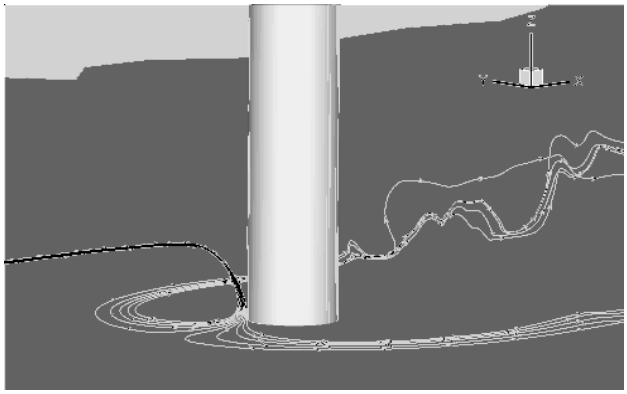

Figure 7. Horseshoe vortex

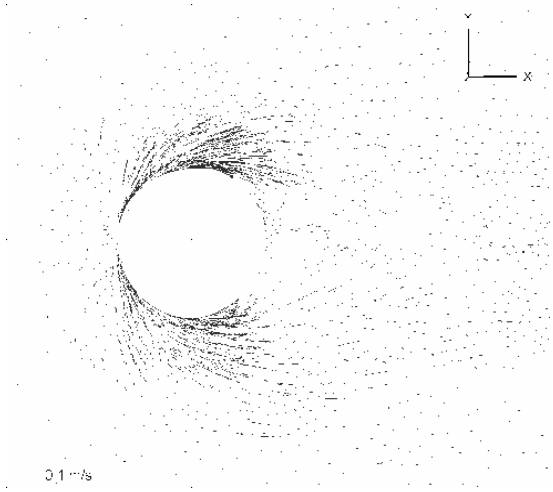

Figure 8. Near-bed Flow Velocities

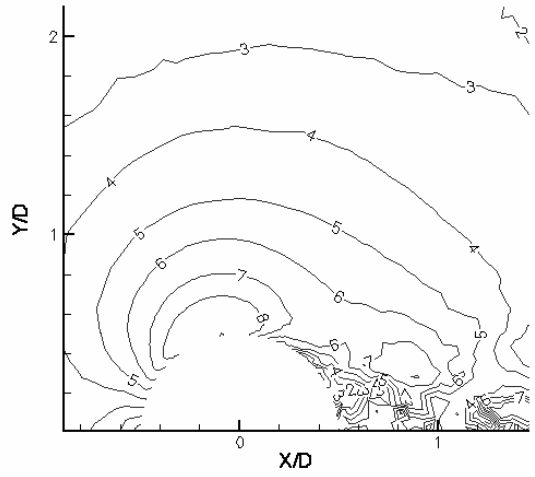

Figure 9. Amplification of Shear Stress

The high shear stresses around the cylinder lead to an intensive sediment transport and therefore the scour develops. Taking into account the transversal sediment transport at a slope leads to a resulting transport vector which no longer points in the direction of shear stress. In Fig. 10 the white arrows denote the direction of shear stress while the grey point in the direction of sediment transport. It can be seen that the latter is less radial after the correction.

After two hours of simulation the scour reaches a depth of approximately 14cm. The temporal evolution (Fig. 11) and the resulting shape of the scour (Fig. 12) are in a good agreement with the experimental results. The scour depth after two hours of simulation is not exactly met.

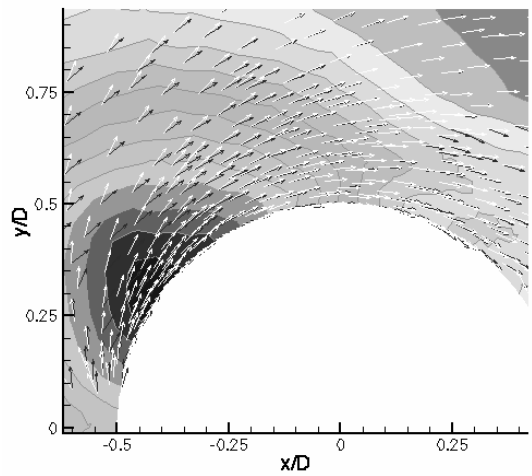

Figure 10. Sediment Transport Rates at a Slope

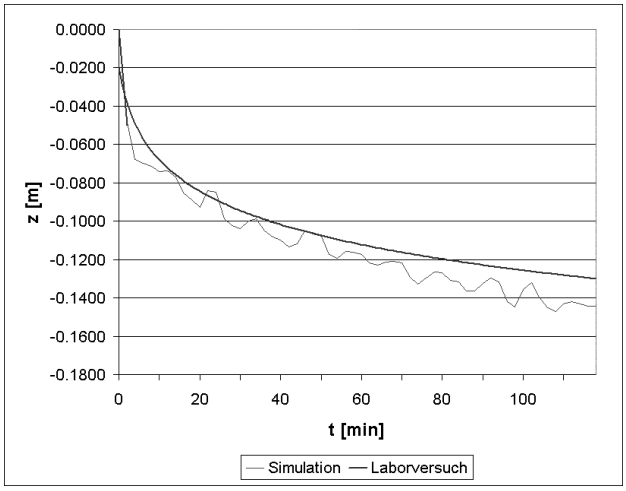

Figure 11. Temporal Evolution of Scour

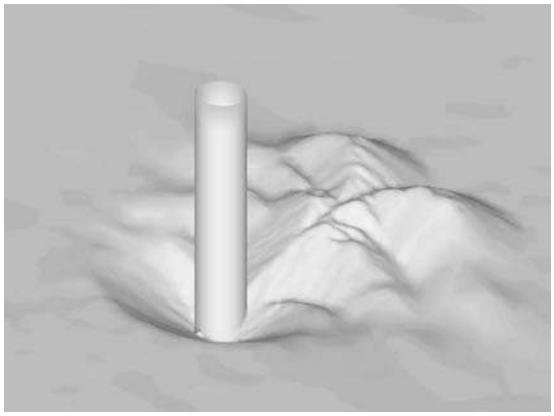

Figure 12. Scour after 2 Hours

B. Bottom

Simulations with the bottom finite element model were carried out in order to analyse the slope stability. At the present state of development the shear stress and dynamic flow pressure have not been taken into account (this will be included in the final version of the paper).

The scour geometry was held constant whereas the friction angle was altered. Other parameters used were Young's modulus $E = 1 \cdot 10^{-4}$ kN/m² and Poisson's ratio $\nu = 0.3$. The unit weight of the material was given as $\gamma = 10 \mathrm{kN/m^3}$. It is assumed that the upper layer is loose sand and therefore cohesion is not effective. After ten minutes of sediment transport the scour has reached a depth of 7cm. For this point in time the finite element simulations were carried out.

The plastic strains γ_{xz} are shown in Fig. 13 and Fig. 14. As a result from experiments in [11] sandslides were initiated when the slope angle was two degrees higher than the friction angle. Fig. 13 shows that with the difference of two degrees between slope and friction angle, strong plastic strains occur on the upstream as well as on the downstream slope. These can be expected to be the areas where most of the sandsliding takes place.

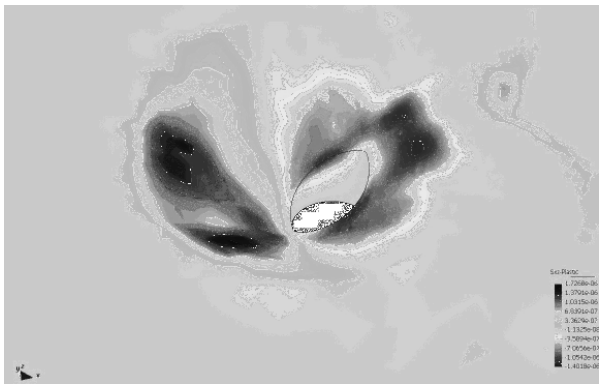

Figure 13. Plastic Strains at $\varphi - 2°$

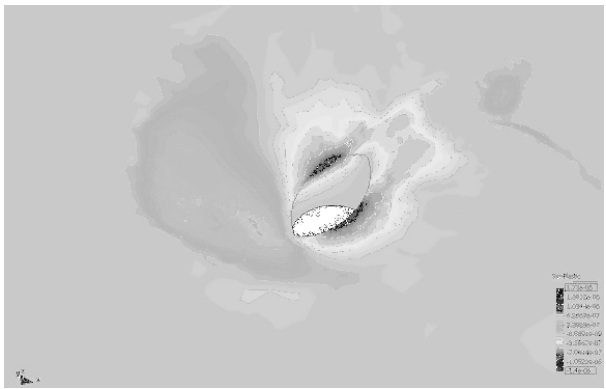

Figure 14. Plastic Strains at φ

IV. SUMMARY

The numerical model described is capable of calculating flow and sediment transport around structures as well as analyzing the bottom stability during scouring with a finite element model. High shear stress in the vicinity of the structure leads to an intensive sediment transport. Steep slopes occur as the scour develops. The change of threshold conditions and sediment transport rates at steep slopes are taken into account by modifying the values for a horizontal bed. Furthermore it is necessary to consider bottom movements which are a result of instabilities and which are independent from shear stress affecting the bottom. The sand slide algorithm is capable of simulating these movements, taken into account the friction angle as the only soil parameter.

The results of the scour simulation met the measured scour depth and the temporal evolution. Using the calculated bottom geometry for an analysis with the finite element model for the bottom leads to information where failure of stability occurs.

REFERENCES

[1] J.S. Damgaard, R.J.S. Whitehouse, R.L. Soulsby, "Bed-load Sediment Transport on Steep Longitudinal Slopes," *J. Hydr. Eng*., Vol. 123 (12), 1997.

[2] F. Engelund, "Flow and Bed Topography in Channel Bends," *J. Hydra. Div*., ASCE, Vol. 100 (11), 1974.

[3] S. Ikeda, "Incipient Motion of Sand Particles on Side Slopes," *J. Hydra. Div*., ASCE, Vol. 108 (1), 1982.

[4] S. Ikeda, "Lateral Bed-Load Transport on Side Slopes," *J. Hydra. Div*., ASCE, Vol. 108 (11), 1982.

[5] S. Ikeda, "Lateral Bed-Load Transport on Side Slopes," In: Civil Engineering Practice 2, Technomic Publishing Company, USA, 1988.

[6] Jacek A. Jankowski, "A non-hydrostatic model for free surface flows," Institute of Fluid Mechanics, University of Hannover, Report No. 56, 1999.

[7] E.W. Lane, "Design of Stable Channels," *Trans*., ASCE, Vol. 120, 1955.

[8] O. Leiner, "Zur Erforschung der Geschiebe und Sinkstoffbewegung," Zeitschrift für Bauwesen, Vol. 62, 1912.

[9] A. Malcherek, F. Piechotta,"Mathematical Module SediMorph," Federal Waterways Engineering and Research Institute, Germany, Technical Report, 2004.

[10] F.R. Menter, "Improved two-equation k-omega turbulence models for aerodynamic flows," NASA technical memorandum 103975, NASA, Ames Research Center, California, 1992.

[11] A. Roulund, "Three-dimensional Numerical Modelling of Flow around a Bottom-mounted Pile and its Application to Scour," Ph.D. thesis, Department of Hydrodynamics and Water Resources, Technical University of Denmark, Series Paper No. 74, 2000.

[12] A. Roulund, M. Sumer, J. Fredsøe, J. Michelsen, "Numerical and experimental investigation of flow and scour around a circular pile," *J. Fluid Mech*., Vol. 534, 2005.

[13] A. Schoklitsch, "Über Schleppkraft und Geschiebebewegung," Leipzig und Berlin, W. Engelmann, 1914.

[14] M. Sekine, G. Parker, "Bed-load transport on transverse slope. I.," *J. Hydr. Eng.* Vol. 118, No. 4, 1992.

[15] A. Shields, "Anwendung der Ähnlichkeitsmechanik und der Turbulenzforschung auf die Geschiebebewegung," Mitt. der Preussischen Versuchsanstalt für Wasserbau und Schiffbau, Vol. 26, 1936.

[16] G.M. Smart, "Sediment Transport Formula for Steep Channels," *J. Hydr. Eng*,. ASCE, Vol. 110, No3, 1984.

[17] I.M. Smith, D.V. Griffiths, „Programming the Finite element Method," John Wiley & Sons Ltd., 3rd Edition, 1998.

[18] M. Sumer, J. Fredsøe, "The Mechanics of Scour in the Marine Environment," Advanced Series in Ocean Engineering Vol. 17, World Scientific Publishing Co. Pte. Ltd., Singapore, 2002.

[19] L.C. van Rijn, "Principles of Sediment Transport in Rivers, Estuaries and Coastal Seas," Aqua Publications, Amsterdam, 1993.

[20] H. Weilbeer, "Numerische Simulation von Strömung und Kolkung an Wasserbauwerken," Institute of Fluid Mechanics, University of Hannover, Report No. 66, 2001.

[21] R.J.S. Whitehouse, J. Hardisty, "Experimental Assessment of Two Theories for the Effect of Bed Slope on the Threshold of Bed Load Transport," *Marine Geology*, Vol 79, 1988.

[22] D.C. Wilcox, "Turbulence Modeling for CFD," DCW Industries, California, USA, 2nd Edition, 1993.

[23] O.C. Zienkiewicz, R.L. Taylor, "The Finite Element Method," Butterworth-Heinemann, Oxford, 5th Edition, 2000.